Exclusive Photodisintegration of ^{3}He with Polarized Photons

D. J. Tedeschi,[3] G. S. Adams,[3] G. Audit,[9] H. Baghaei,[8] A. Caracappa,[1] W. B. Clayton,[3] A. D'Angelo,[4] M. A. Duval,[6,*] G. Giordano,[2] S. Hoblit,[8] O. C. Kistner,[1] J. M. Laget,[9] R. Lindgren,[8] G. Matone,[2] L. Miceli,[1] W. K. Mize,[6] M. Moinester,[7] C. Ruth,[3] A. Sandorfi,[1] C. Schaerf,[4] R. M. Sealock,[8] L. C. Smith,[8] P. Stoler,[3] P. K. Teng,[3,5] C. E. Thorn,[1] S. T. Thornton,[8] K. Vaziri,[3,†] C. S. Whisnant,[1,6] and E. J. Winhold[3]

[1]*Physics Department, Brookhaven National Laboratory, Upton, New York 11973*
[2]*Istituto Nazionale di Fisica Nucleare-Laboratori Nazionali di Frascati, Frascati, Italy*
[3]*Physics Department, Rensselaer Polytechnic Institute, Troy, New York 12180-3590*
[4]*Istituto Nazional di Fisica Nuclear and University of Rome Tor Vergata, Via della Ricerca Scientifica, 00133 Rome, Italy*
[5]*Institute of Physics, Academia Sinica, Taipei, Republic of China*
[6]*Department of Physics, University of South Carolina, Columbia, South Carolina 29208*
[7]*School of Physics and Astronomy, Tel-Aviv University, 69978 Tel-Aviv, Israel*
[8]*Physics Department, University of Virginia, Charlottesville, Virginia 22903*
[9]*DAPNIA/SPhN CE-Saclay, 91191 Gif-sur-Yvette, Cedex, France*
(Received 10 February 1994)

The first measurement of exclusive photodisintegration of ^{3}He with polarized photons is reported. Cross sections and asymmetries for $^3\mathrm{He}(\vec{\gamma},pn)p$ and $^3\mathrm{He}(\vec{\gamma},pp)n$ at $235 \leq E_\gamma \leq 305$ MeV are compared to a theoretical calculation which includes one-, two-, and three-nucleon photon absorption. Two-nucleon absorption dominates the *pn* data, but is suppressed in the *pp* data. The *pp* data require the inclusion of three-nucleon absorption to describe the cross section and beam asymmetry over all momenta.

PACS numbers: 25.20.Dc, 25.10.+s, 27.10.+h

Understanding nuclei in terms of baryonic and mesonic fields is one of the primary goals of nuclear physics. Photonuclear reactions play a fundamental role in this effort because the photon coupling strength to nucleon and subnucleon degrees of freedom is well known [1,2]. Recent work on the photodisintegration of ^{3}He has concentrated on elucidating the photoabsorption mechanisms at intermediate energies [3]. Measurements of inclusive and exclusive cross sections suggest that a substantial fraction of the total photodisintegration cross section proceeds through the three-nucleon absorption channel [4–7]. Similar studies of pion absorption on ^{3}He have shown that three-nucleon mechanisms are significant in those reactions as well [8–10].

The aim of the present experiment was to explore exclusive photodisintegration of ^{3}He over a wide kinematical acceptance, and use the beam polarization asymmetry to provide a detailed test for models of three-body breakup. This Letter reports the first measurement of the coincidence reactions $^3\mathrm{He}(\vec{\gamma},pn)p$ and $^3\mathrm{He}(\vec{\gamma},pp)n$ using linearly polarized photons. Momentum distributions of the differential cross section and beam asymmetry at a proton emission angle of 100° are presented, along with angular distributions for $^3\mathrm{He}(\vec{\gamma},pp)n$.

The experiment was performed at the LEGS polarized photon facility located at the National Synchrotron Light Source at Brookhaven National Laboratory [11]. Compton backscattering of ultraviolet laser light produced photons in the energy range $200 \leq E_\gamma \leq 305$ MeV with a resolution of 6 MeV FWHM. The photon energy for each event was determined by detecting the recoiling electron in a magnetic spectrometer. The resulting tagged-photon intensity was 2×10^6/sec. Multiple tagger hits were rejected in the analysis, resulting in a ninety percent tagging efficiency. Beam flux was continuously monitored with e^+e^- pair creation detectors located downstream of the target. Beam polarization was calculated using the measured value of the laser polarization and the kinematics of Klein-Nishina scattering. The polarization ranged from 0.73 at low energies to 0.99 at the highest energies. The photon beam was incident upon a 10 cm long Ni cell (5 cm diameter, with 0.012 cm wall thickness) containing liquid ^{3}He. A constant temperature of 3.1 K ensured a stable density of 0.062 g/cm^3. The beam profile on target was approximately elliptical with major and minor axes of 4 and 2 cm, respectively. Data were taken alternately with the target cell full and empty in order to subtract background contributions from the cell walls.

Proton telescopes consisting of plastic scintillator and CaF_2 (phoswich) were placed below the beam at proton (p_1) angles $20° \leq \theta_{p_1} \leq 160°$, at 20° intervals (see Fig. 1). Three telescopes having a total solid-angle coverage of 0.062 sr were located at each angle. Correlated E(plastic) and $\Delta E(CaF_2)$ information was used for particle identification. The proton energy resolution was typically 6% FWHM and a momentum threshold of 300 MeV/c was set in software. The phoswich detectors were calibrated by measuring protons from the two-body breakup of deuterium over the full range of tagged photon energies. To calibrate the low energy response, deuterons from the two-body breakup of ^{3}He were also measured. Proton counting inefficiencies were determined by a GEANT [12] simulation

0031-9007/94/73(3)/408(4)$06.00

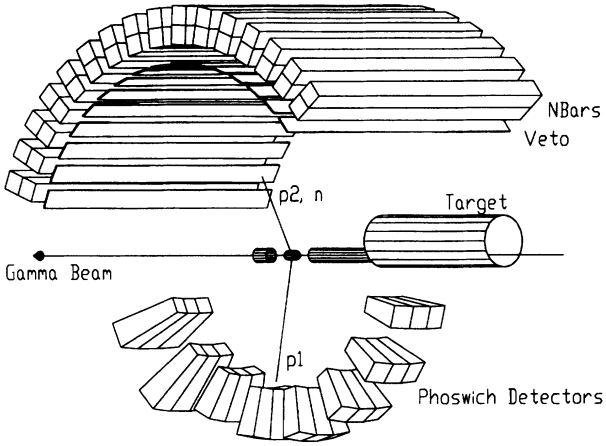

FIG. 1. Experimental apparatus. The lower scintillator array detected protons (p_1) and the upper array detected protons (p_2) or neutrons (n).

of the experimental cuts and the data were corrected on an event-by-event basis.

Two layers of $160 \times 10 \times 10$ cm^3 scintillation counters made of BC-408 plastic scintillator were used to detect protons (p_2) and neutrons (n) in coincidence with protons (p_1) in the phoswich detectors. Thin scintillators in front of the array ("veto" in Fig. 1) were used for charged particle identification. Each detector was viewed by a photomultiplier tube at each end. The signals from each end were used to calculate particle time of flight (TOF) and position along the bar, and hence the particle momentum. The resulting TOF resolution was 0.6 ns FWHM, and the position resolution was 5 cm FWHM. These detectors covered the angle range $24° \leq \theta_{p_2,n} \leq 144°$. With cuts on the azimuthal angle relative to the $\vec{\gamma}$-p_1 plane, $-30° \leq \phi_{p_2,n} \leq 30°$, a total solid-angle coverage of 1.25 sr was achieved for all the data reported here. Neutrons from the photodisintegration of deuterium provided timing and position calibration. A software threshold for proton and neutron detection was set at 300 MeV/c to insure little variation of neutron detection efficiency due to gain drift in the photomultiplier tubes and to provide symmetry between the pn and pp triggers. The neutron efficiency was calculated using the Kent State code [13]. Data that passed a missing mass cut were corrected on an event-by-event basis. The accuracy of the calculated efficiency is expected to be about $\pm 5\%$. The absolute efficiency was confirmed at two angles by comparing the rate from deuteron photodisintegration in single-arm and coincidence measurements using the same apparatus. The measured efficiencies agreed with the calculated values within the $\pm 8\%$ uncertainties in the measurements.

Figure 2 shows the cross section and asymmetry for the pp (solid squares) and pn (open circles) measurements at $\theta_{p_1} = 100°$, integrated over the full acceptance (momentum and solid angle) in p_2 or n. Statistical er-

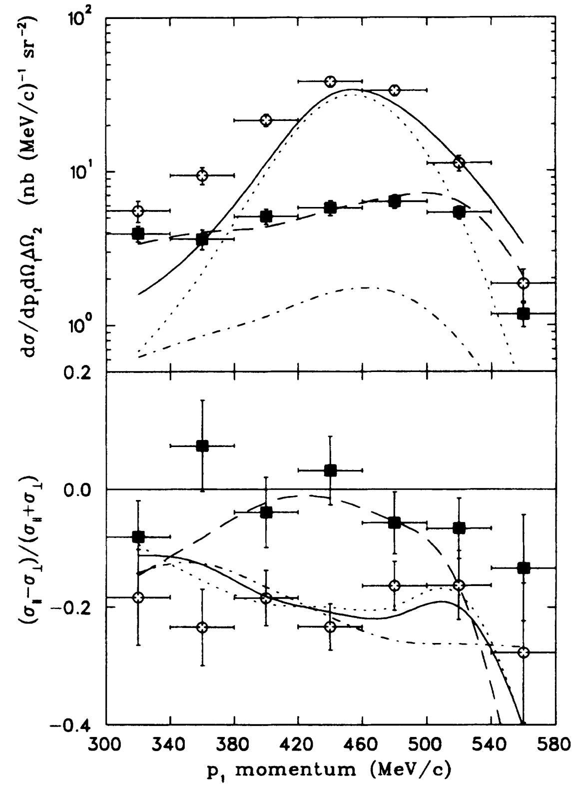

FIG. 2. Comparison of pp and pn cross sections and asymmetries for $235 \leq E_\gamma \leq 305$ MeV: solid squares, ^{3}He($\vec{\gamma}, pp$)n; open circles, ^{3}He($\vec{\gamma}, pn$)p. The dotted (pn) and dot-dashed (pp) lines are theoretical predictions which include $1N + 2N$ absorption. The solid (pn) and dashed (pp) lines are for the full calculation.

rors combined with uncertainties in detector efficiency are shown in the figures. The systematic error in the absolute cross section arising from uncertainties in detector solid angles, photon flux, and reaction losses in the scintillators is $\pm 5.5\%$. The pn cross section peaks around p_1 momentum equal to 440 MeV/c. The pp cross section is much lower than the pn cross section at this momentum. This reflects the fact that the pn data are dominated by a large quasideuteron component, while the analogous mechanism for the pp channel is suppressed because the diproton has no dipole moment and charged meson-exchange currents are not allowed [3]. Similar features were observed in the data at other angles. The asymmetry for the pn data is negative and consistent with that of deuteron photodisintegration [14] while the pp asymmetry is close to zero. It should be noted that the division of the data into pn and pp triggers merely emphasized different regions of phase space for the final state nucleons. The pn (pp) triggers tend to select large opening angles for the pn (pp) pairs.

The theoretical curves in Figs. 2 and 3 are predictions of a multiple scattering calculation [15] which includes one- ($1N$), two- ($2N$), and three-nucleon ($3N$) absorption

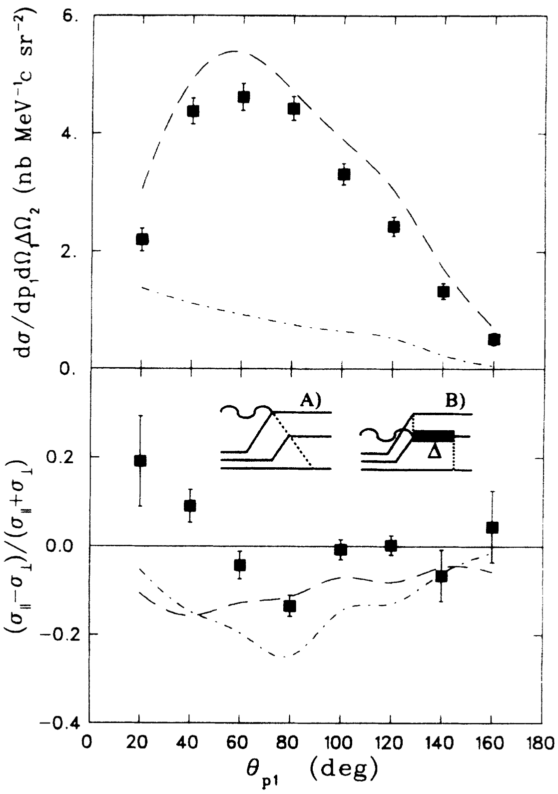

FIG. 3. Cross sections and asymmetries for $^3\mathrm{He}(\vec{\gamma},pp)n$ at $270 \leq E_\gamma \leq 305$ MeV, and $p_1 \geq 300$ MeV/c. The dot-dashed curve is the theoretical result for $1N$ and $2N$ absorption only. The dashed line is the full calculation including $3N$ absorption (insets A and B).

mechanisms. The $1N$ and $2N$ operators have been used previously to describe the main features of pion production from deuterium [16] and deuteron photodisintegration [17]. The $3N$ currents include meson double scattering [18], and double-pion production through an intermediate delta [2,6]. The present results change only slightly when the double-pion graph (inset B in Fig. 3) is omitted from the calculations. Final-state interactions (FSI) are included for all absorption mechanisms. The FSI are treated in a truncated multiple-scattering series using the Paris potential.

This theoretical model is able to account for the inclusive proton cross section for ^{3}He in the $\Delta(1232)$ energy region [4,5]. It does not do as well in describing the published coincidence data [6,7,19]. The choice of in-plane kinematics for the previous photodisintegration measurements resulted in extreme sensitivity to the treatment of FSI. Since the present data are integrated over a large region in three-nucleon phase space, less sensitivity to FSI is expected.

Figure 2 shows a comparison of the theoretical results with the pn and pp data at 100°. In each case, the theory was integrated over the full acceptance of the experiment by Monte Carlo methods. Events were randomly selected in p_1 and p_2 within the experimental ranges of momenta and angles, then weighted according to the theoretical cross section. Events which passed the data cuts were included in the calculation of the average cross sections. This process was carried out until the results for each datum exhibited statistical uncertainties no larger than $\pm 4\%$. The method was checked by reproducing the theoretical results in Ref. [6]. Theory gives a good account of the large ratio of pn to pp cross sections at proton momenta around 440 MeV/c. At this momentum the pn cross section and beam asymmetry are determined primarily by photon absorption on a pn pair, the quasideuteron effect. When $3N$ amplitudes are included in the calculation, the cross section is affected only at extreme momenta above and below the quasideuteron peak. Overall agreement with the measured cross sections is very good except at low momentum, where the predicted cross sections are about a factor of 3 low. Theory is in accord with the pn asymmetry data, with the $3N$ amplitudes changing the predictions slightly.

The pp data exhibit a very different sensitivity to the competing reaction mechanisms than the pn data. Theoretical predictions including $1N$ and $2N$ amplitudes alone fail to account for the measured pp cross section or asymmetry. The theoretical cross sections are about a factor of 5 too low. This is primarily the result of a suppression of the $2N$ amplitudes for pp absorption over those for pn. Absorption on a pn pair followed by FSI can also result in the detection of two energetic protons, but these channels are included in the calculation and they produce cross sections which are too small (see Fig. 2). Also, the predicted asymmetries for $1N + 2N$ absorption resulting in pp coincidences are negative, lying close to those for the pn measurement while the data show values near zero. Adding $3N$ absorption to the theory produces results which are in very good agreement with the data.

In the theory (dashed curve in Fig. 2) the shape of the momentum distribution for pp events is dictated by a large contribution from the $3N$ mechanism which produces a π^+ on a proton, followed by π^+ absorption on a pn pair. This meson-rescattering diagram results in a broad peak in the cross section at high momentum, in agreement with the data. The theoretical results including $1N$ and $2N$ amplitudes alone (dot-dashed curve) show a similar peak but with a cross section which lies far below the data. One might argue that the uncertainties in the $2N$ model (from the choice of NN potential, for example) allow for some adjustment in the overall normalization of the $2N$ cross section. However, the present asymmetry data preclude any modification of the theoretical model which strongly enhances the $2N$ component.

Figure 3 shows the angular distributions for the pp events integrated over the experimental acceptance for p_2. Only data at the highest beam energies, $270 \leq E_\gamma \leq 305$ MeV, are included in the graph. The experimental cross sections show a broad peak which is consistent with the predictions of the $3N$ model. The theoretical values lie above the data at all angles however. The predictions with $1N$ and $2N$ amplitudes alone produce values which are forward peaked and very low in magnitude.

The measured beam asymmetries are small, starting at 0.19 ± 0.10 at 20° and monotonically decreasing to -0.14 ± 0.02 at 80°. The data at larger angles are consistent with zero. One should note that the asymmetry is not constrained to go to zero at 0° and 180° as for a two-body reaction. Theoretical results for $1N + 2N$ amplitudes lie well below the data except at the extreme backward angles. The addition of $3N$ amplitudes significantly improves the agreement with the data at the middle angles, but still fails to reproduce the positive asymmetries at forward angles. The origin of this discrepancy is not known, but we can speculate that the method of including final-state interactions is at fault. The experimental phase-space acceptance for small-angle p_1, at low momentum, is largest when p_1 and n have a small opening angle and low relative momentum, thus enhancing the effects of FSI. This approximate correlation disappears as the angle of p_1 increases. Extensive modifications to the theoretical computer code are needed to study the effects of FSI. These results will appear in a later analysis of the full data set.

In summary, the first measurements of exclusive nuclear photodisintegration with polarized photons have been reported. The experimental division of the ^{3}He data into pn and pp triggers emphasizes different reaction mechanisms. The pn data contain contributions mainly from $2N$ absorption on a pn pair while the pp data are dominated by $3N$ mechanisms. Both the cross section and asymmetry are sensitive to the presence of $3N$ mechanisms. Meson rescattering dominates the pp predictions, with small contributions from double pion production. The failure of the present theory to predict the forward-angle data indicates that further refinements of the model are needed.

This work was supported by the U.S. Department of Energy under Contract No. DE-AC02-76-CH00016, the National Science Foundation, the Instituto Nazionale di Fisica Nuclear, and the U.S.-Israel Binational Science Foundation.

*Present address: Institut de Physique Nucleaire, 91406 Orsay Cedex, France.

†Present address: Fermilab, MS 119 ES&H, Box 500, Batavia, IL 60510.

[1] J.F. Mathiot, Phys. Rep. **173**, 63 (1989).
[2] J.M. Laget, Nucl. Phys. **A497**, 391 (1989).
[3] J.M. Laget, Few-Body Syst., Suppl. **2**, 126 (1987).
[4] N. d'Hose *et al.*, Phys. Rev. Lett. **63**, 856 (1989).
[5] C. Ruth *et al.*, Phys. Rev. Lett. **72**, 617 (1994).
[6] G. Audit *et al.*, Phys. Rev. C **44**, 575 (1991); G. Audit *et al.*, Phys. Lett. B **312**, 57 (1993).
[7] A.J. Sarty *et al.*, Phys. Rev. C **47**, 459 (1993).
[8] G. Backenstoss *et al.*, Phys. Lett. B **222**, 7 (1989).
[9] L.C. Smith *et al.*, Phys. Rev. C **40**, 1347 (1989).
[10] S. Maytal-Beck *et al.*, Phys. Rev. Lett. **68**, 3012 (1992).
[11] C.E. Thorn *et al.*, Nucl. Instrum. Methods Phys. Res., Sect. A **285**, 447 (1989).
[12] R. Brun *et al.*, GEANT3 (Program Library, CERN, Geneva, Switzerland, 1987).
[13] R. Cecil, B. Anderson, and R. Madey, Nucl. Instrum. Methods **161**, 439 (1979); R. Madey (private communication).
[14] L. Miceli *et al.*, contribution to the Particles and Nuclei International Conference, Perugia, Italy, June 1993 (unpublished); L. Miceli *et al.*, Phys. Rev. Lett. **67**, 1206 (1991).
[15] J.M. Laget, Phys. Rep. **69**, 1 (1981).
[16] P. Bosted and J.M. Laget, Nucl. Phys. **A296**, 413 (1978).
[17] J.M. Laget, Can. Phys. **62**, 1046 (1984).
[18] J.M. Laget, J. Phys. G **14**, 1445 (1988).
[19] N.R. Kolb, Phys. Rev. C **44**, 37 (1991).